JOURNAL OF
MEDICINAL
CHEMISTRY

Volume 36, Number 23 November 12, 1993

Articles

On the Mechanism of HRV-14 Antiviral Compounds: "Slow Growth" as a Conformational Search Procedure

Michael Guha-Biswas, Michael Holder, and B. Montgomery Pettitt*

Department of Chemistry, University of Houston, Houston, Texas 77204-5641

Received February 12, 1993•

We report a novel conformational search procedure that is used to investigate the binding mechanism of a member of the WIN class of antiviral compounds. A simple hypothesis of important residues in the binding site based on differences in drug-free and drug-bound X-ray structures along with more elaborate models, ultimately including the entire virus, is considered. Our search method is a variant of slow-growth molecular dynamics used in free energy simulations and gives rise to local motion in the protein backbone of up to 3 Å. This technique involves the scaling of drug–protein interaction energies over time periods of 10–100 ps and gives rise to local motion in the protein backbone. In addition, we have used high-temperature dynamics with periodic quenching to generate low-energy conformations with backbone displacements in the crystallographic binding region of up to 7 Å from the native structure. Mechanism of binding, hydrogen-bond stabilization of active-site conformations, concerted drug–protein motions, and the mode of virion stabilization are addressed in relation to our ligand induced and high-temperature conformational search procedures. A loop-cap like mechanism is consistent with the results of our study. A large movement of the "active-site" residues is shown to be theoretically possible and provides a greater access for entry of the drug into its binding pocket than seen in the available crystal structures.

Introduction

The picornaviruses are a large family of viral pathogens that cause disease in both humans and animals. Phylogenetically subdivided into four genera, the picornaviruses are classified according to their buoyant density, pH stability, and sedimentation coefficients. The four classes are (1) enterovirus, which includes polio, hepatitis A and coxsackie viruses; (2) cardiovirus, which includes the encephalomyocarditis and mengo viruses; (3) apthovirus, which includes the foot-and-mouth disease virus, or FMDV; and (4) rhinovirus (common cold virus). The gene sequences of HRV, FMDV, poliovirus, and encephalomyocarditis virus are highly homologous; HRV and poliovirus, in fact, show almost complete sequence homology.[1]

One interesting feature of the picornaviruses is their variable response to different antibodies. Poliovirus has three known serological types, or serotypes, foot-and-mouth disease (FMDV) has seven, yet human rhinovirus (HRV) has no less than 89 and probably more than 100.[1,2] It is therefore not feasible to administer a vaccine for the common cold, because one vaccine would only confer resistance to a small number of the many different cold virus strains.

A class of compounds (first synthesized at the Sterling Winthrop Research Institute, hence coded WIN) was found to show broad-spectrum antipicornavirus activity.[3] One compound in particular, 5-[[4-(4,5-dihydro-2-oxazolyl)-phenoxy]alkyl]-3-methylisoxazole, WIN 51711, has been the subject of pharmacological studies. The mode of action of this compound has been shown to be consistent with the inhibition of viral uncoating,[4] and it is believed that many of this class of compounds prevent uncoating without altering cellular recognition and internalization through the cell membrane. While a complete understanding of

• Abstract published in *Advance ACS Abstracts*, October 1, 1993.

0022-2623/93/1836-3489$04.00/0

the mode of inhibition of the WIN compounds is still the subject of study, two hypotheses have been proposed:[3] (1) a locking or stiffening of the viral protein may occur through specifically modified fluctuations or (2) the drug may block the flow of ions entering the viral interior through a pore on the floor of the canyon. A large channel, which lies beneath the binding site and leads to the RNA interior, is a postulated ion channel that may play a role in the pH-mediated uncoating process. The WIN compound is situated in the viral protein matrix in such a way as to possibly interfere with the flow of ions and water through this channel.[5] Certainly, these explanations are not mutually exclusive.

The details of the binding mechanism of these compounds to the viral coat has been far less studied. As yet, structures of two states, drug-bound and unbound, are known for the protein coat.[2,6] In the drug-bound state only a small portion of the drug is not covered by the protein structure. The intermediate states involved in the mechanism of binding are not revealed as yet by crystallography. In this paper we consider structural fluctuations that may be related to the possible mechanisms of binding of the class of compounds.

Structure–activity studies performed with various analogues of the WIN compound have been used to characterize specific drug–protein affinities. Structure–activity studies involve the modification of a moiety of the drug being tested and subsequent trial, in this case through viral plaque growth.

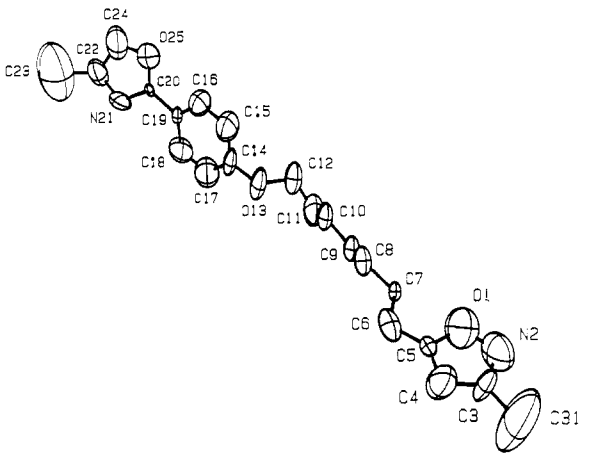

The drug's orientation in this hydrophobic pocket is such that the oxazoline and phenoxy rings (OP group) are roughly coplanar, and the isoxazole end (I group), which forms the other end of the drug, is separated from the OP end by the almost fully extended seven-membered aliphatic chain.[2] In WIN 51711, the OP group is found in the relatively hydrophilic area that lies close to the pore leading into the RNA interior, while the I group fits snugly into the interior of the β-barrel, which is the more hydrophobic area of the binding site. It should be noted that the members of the drug family may bind in either this or the antiparallel orientation.[6] In the orientation for WIN 51711 revealed by X-ray studies, a drug nitrogen WIN N21 in the oxazoline ring lies in close proximity to a polar residue VP1 Asn-203, suggesting that a hydrogen bond here serves to orient the OP end of the WIN compounds in the pocket. This hydrogen bond does not, however, impart much in the way of equilibrium stability as shown by previous theoretical considerations.[7]

The crystal coordinates of the ligated (holoprotein) and unligated (apoprotein) structures differ mainly in a region of about 15 residues. Comparison shows that the conformational difference occurs in the region connecting the βH strand with the FMDV loop region (VP1 196–210).[3] Backbone changes occur in this overlap region of up to 4.5 Å, and even greater side-chain movements are found. His-204, which is exposed at the bottom of the canyon, undergoes the largest shift, which seems to allow access of the I end to the hydrophobic end of the binding site. (The two residues VP1 198 and 206, which are both glycine residues, seem to be the "pivot points" of the drug-induced displacement.) Other apo–holo differences include smaller conformational changes, which are observed in residues lying underneath the binding site. Only a small part of one end of the drug is exposed in the holo structure which thus provides few hints on the mechanism of drug binding.

The chirality of a methyl moiety attached to the oxazole ring has also been shown to have a significant equilibrium effect.[3] This is apparently due to a favorable hydrophobic contact with Leu-90 and Ser-91 in the *R* enantiomer. This may stabilize, in turn, the hydrogen-bond interaction between its neighboring atom N21 and Asn-203. Such studies naturally assume that the binding component is the dominant factor in the MIC values. More quantitative comparisons will have to await definitive correlations between drug structure and inhibition of viral replication via the associated MIC value with binding constants for a particular compound.[5,8]

Thermodynamic integration (TI) and thermodynamic perturbation (TP) theory have been applied to various systems[7,9–12] to calculate relative free energies of solvation and to calculate relative Helmholtz free energy differences of binding in drug–protein complexes. Direct calculation of ΔA or ΔG[13] in a ligand–receptor complex, however, is fraught with difficulty due to poor numerical (statistical) convergence; these problems are often avoided by application of a thermodynamic cycle method to calculate $\Delta\Delta A$ rather than ΔA values. TI methods of relative $\Delta\Delta A$ calculation have recently been successfully extended to a HRV-14/WIN system, but only for small changes such as a single moiety of the drug or mutation of a single residue close to the drug.[12] Large changes associated with ΔA still present difficulties in sampling for these methods. In studying a different aspect of this system, we shall use the slow-growth variant of thermodynamic integration compared and contrasted with high-temperature-quenched dynamics as a way of probing some of the conformational space between the drug-bound (holo) and unbound (apo) states of the virus.

Time-scale limitations make it infeasible to "pull" or "grow" a drug into its observed binding site and observe the relaxation that occurs in the actual binding process. Through recent developments in molecular dynamics simulation techniques,[9,14] however, aspects of such a process can be modeled. These techniques have been used here to study the conformational migrations involved in the binding of the isoxazole class of antiviral agents to HRV-14.[8,15] The convergence of these calculations is problematic in obtaining free-energy differences for the overall drug binding process.[9] Therefore, we have not attempted to obtain thermodynamic results. Instead the presence of forces caused by varying the strength of the drug–virus interaction is used in an attempt to move the conformational state(s) of the system from the unbound

form to the drug-bound form and vice versa. Slow-growth methods are thus exploited to gradually add the protein–ligand interaction potential into the total system energy. This constitutes a conformational search of the structural changes that occur in the surrounding protein environment. In addition, to probe structural changes with activation barriers that are many times thermal energy at room temperature, high-temperature simulations with either quenching or annealing may be used as a conformational search aid.[20] We consider the slow growth and quenching methods individually and in combination to search the conformational space of HRV-14 between the two observed crystallographic states. It is our hope that these methods of ligand-based and high-temperature conformational searching will be used to augment the investigation of drug–protein interactions through extensive molecular dynamics simulations.[19]

Methods

The first step in our procedure was to create a "hybrid" (nonphysical) structure comprised of the drug coordinates taken from the drug-bound (holo) X-ray crystallographic structure of the viral capsid protomer and protein coordinates from the native (apo) structure. In the native apoprotein structure, the coordinates of symmetry-related protomers were generated so that all atoms within 25 Å of Cβ Val-188 were included in the coordinate set used for calculations.[18] The region of closest approach in the hybrid structure was around residue Met-205 of subunit VP1, where contacts of 0.76 and 0.91 Å were created between Cβ of Met-205 and WIN atoms C12 and O13, respectively. The nonbonding (van der Waals) energies alone for this distance approach was 10^9 kcal/mol. In ordinary molecular modeling these contact distances could be decreased to normal values through energy minimization, but in this case the nonbonded energy is intentionally propagated to selected regions of the surrounding protein matrix.

The simulations described herein involve the standard calculation of a molecular dynamics trajectory, but with the difference that a scaling parameter, λ, is applied to all drug–protein interaction energies. The scaling parameter, λ, was varied from 0 (actually 10^{-8}) to 1.0 using the "slow-growth" method[9] with a scaling power of 2 (i.e. λ^2). This proved to be effective in providing gentler initial conditions as well as increasing the conformational sampling in the $\lambda = 10^{-4}$ to 10^{-1} range. As an example, a value of $\lambda = 10^{-8}$ would scale a nonbonded potential of 10^9 to a realistic range (1–10 kcal/mol) and cause a slight repulsive effect while still allowing sufficient time for the protein environment to "adjust" to the induced perturbation. As the interatom distances approach the sum of the normal van der Waals radii, the repulsive effect would decrease and normal dynamical forces would supervene. The molecular dynamics parameters used in calculating the trajectories were based on standard methodology[14] and are as follows. We used an 8.0-Å nonbonded cutoff and a time step of 1 fs. The equations of motion were integrated using the Verlet algorithm,[17] and to maintain a constant temperature, velocities were scaled in a window of ±10 K at all the temperatures of interest –300, 1000, or 2000 K. The high temperatures were used to facilitate barrier crossings to search for other low-energy conformations. Both a constant dielectric of 1.0 and a distance-dependent dielectric treatment of solvent environment were used as specified below.

Using an energy-minimized but unequilibrated crystallographic structure introduced the possibility that small localized increases in atomic fluctuations might be confused in the analysis with the growing forces of the drug moieties from the slow-growth procedure. For this reason our structural comparisons compare the dynamical structure (with slow growth of ligand) versus the control structure (the same dynamic simulation without slow growth) rather than simply a comparison of the initial and final structures of a particular trajectory. Slow growth in a fully equilibrated protein structure[19] was performed for purposes of comparison, but the choice of using the unequilibrated coordinates was arbitrary.

Our simulations are categorized based on the number of atoms that are configurationally constrained to their reference (initial) positions. This approach was dictated by the computational expense of modeling the 7000 heavy-atom capsid icosahedral protomer unit surrounded by its symmetry related neighbors.

In our first model (model 1), all atoms of the hybrid structure except those of the FMDV loop region (VP1 196 to VP1 210) were fixed. A listing of these residues from 196 to 210 is as follows: Gln-Tyr-Gly-Ile-Thr-Val-Leu-Asn-His-Met-Gly-Ser-Met-Ala-Phe. This "string" of residues proved to be a convenient dynamic "active-site" model hypothesis for the first level of trials, and since most of these residues are exposed to the surface, their movement was relatively unrestrained. The zone of unconstrained atoms was then increased to all atoms within 10 Å of any atom of the drug (model 2). Since drug–protein atomic interactions are thus free on all sides of the drug, movement of residues underlying the binding site is expected. Finally, the full virion with icosahedral boundary conditions was considered (model 3); theoretically the most realistic model, slow-growth forces would be propagated throughout the viral capsid. A sequential-growth model, in which the drug atoms were scaled individually, in topological sequence, was approximated by introducing new fragments of the drug and scaling each atomic addition in sequence; the procedure followed was otherwise the same with the exception that velocities were periodically reassigned.

Using our model 1, additional slow-growth simulations were performed to elucidate some aspects of model-dependent solvent effects, hydrogen bonding in the active-site region, and conformational sampling limitations. These included:

(1) A 10-ps slow-growth simulation in which the presence of solvent was approximated by using an r-dependent dielectric rather than a constant dielectric.

(2) A 50-ps simulation performed at a higher temperature (1000 K).

(3) A 50-ps simulation in which the number of intraloop hydrogen bonds formed between atoms of residues VP1 196 and 210 as well as hydrogen bonds between these residues and the drug were monitored.

(4) 10-, 50-, and 100-ps simulations in which the degree of displacement was correlated with simulated duration. Simulations 3 and 4 above were performed using a previously equilibrated apoprotein structure.[7]

It was noticed that if the drug atoms were not configurationally constrained, scaling of the bond potential caused large atomic excursions and consequent deformation of the drug at low values of λ. At $\lambda \geq 0.1$ the bond potential is sufficiently high to maintain the drug's physical integrity. We describe one simulation using model 3 in which the drug is freed from fixed atom constraints at $\lambda = 0.1$ and allowed to equilibrate with the protein for 10 ps.

Quenched molecular dynamics simulations (high-temperature configuration minimizations) involve the assignment of velocities at a higher temperature (e.g. 2000 K) to a selected set of atoms (e.g. residues 196–210 for model 1), calculation of a trajectory, and quenching (minimizing) periodically to generate a number of conformations that presumably represent those that could be sampled in this case by the residues around the drug at some time during the binding event. If combined with slow growth, the possibility of finding new atomic drug–protein interactions arises. We have thus performed quenching simulations in the presence (with slow growth) and absence of the drug. Over a duration of 50 ps, structures were selected and minimized (quenched) from 2000 K by 1500 steps of steepest descent and 3000 steps of adopted basis Newton–Raphson minimization, which ensured a ΔE per step of less than 0.001.

Results

A 10-ps trajectory was calculated with model 1 constraints. The ligand-induced movement was evident, and the displacement was, not surprisingly, centered around residue 205 where the closest contacts were present. A significant event was the occurrence of a ring flip of the imidazole ring of residue 203 His, which was obviously coupled to the abrupt side-chain movement of residue 204 Met. This event was not observed in the control and was,

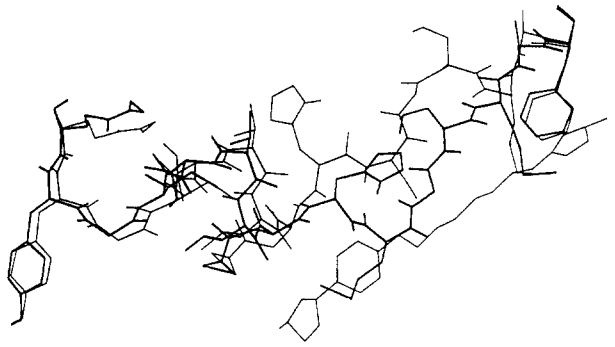

Figure 1. Comparison of the final structures of a 50-ps trajectory with (light) and without (dark) slow growth in model 1. Atoms of residues 196–210 and the WIN compound are shown. Adjacent explicit hydrogens appear "bonded" (as triangles) here and below.

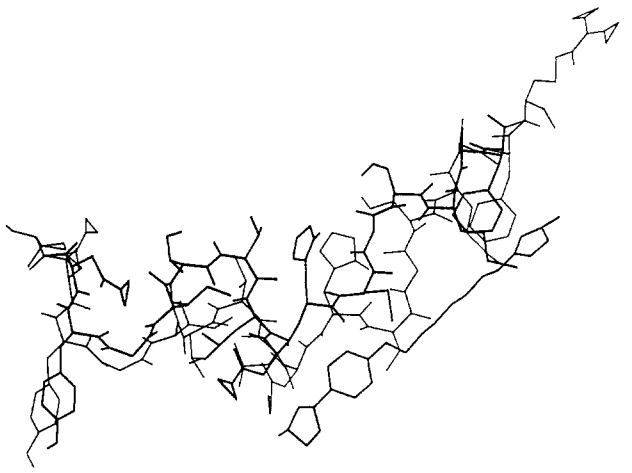

Figure 2. Comparison of the final structures of a 20-ps trajectory trajectory with (dark) and without (light) slow growth in model 2. (Atoms of residues 196–210 and the WIN compound are shown.)

in part, a result of the growing nonbonded interactions between the close contact atoms. The ring adopted a plane parallel to that of the same imidazole ring in the holo structure. When repeated for longer times of 50 and 100 ps, no ring flips were observed, but greater backbone displacements (up to 3 Å) and larger side-chain motions were observed. Over 50 ps, displacement of the residues 204–208 evolved further while that of residues 198–203 remained limited (see Figure 1), because a hydrogen bond cluster of 4–6 hydrogen bonds stabiiized the 199–203 region. Thus, with the model 1 constraints, slow growth could induce backbone displacement only in regions that lacked a particular level of stabilization, in this case provided by hydrogen bonds. To measure the capacity of slow growth to induce the empirically observed apo to holo transition, the root mean square difference between atoms of residues 196–210 of the final dynamical and crystal holo structure was calculated. In this case after 50 ps, it was 2.6 Å.

Increasing the unconstrained zone to within 10 Å of any atom of the drug (model 2), a 20-ps trajectory was performed. Movement in the 196–210 region was similar to that found in model 1, but displacement of all remaining residues impinging on the binding site occurred as expected (see Figure 2). In contrast to model 1, a shift of Ile-199 Cα of 2.3 Å, where previously it was less than 0.8 Å, was observed. The residues 199–203 lost the hydrogen-bond stabilization found in model 1, but residues 203 and 204 still showed decreased displacement. This might reflect an inherent affinity between the oxazole end of the drug and residue 203 or 204. The final rms difference between the dynamical and the holo structure loop atoms (196–210) was 2.58 Å.

The application of slow growth to the entire virion (model 3) using icosahedral boundary condition molecular dynamics showed a delocalized set of structural effects, with the perturbation being largely distributed throughout the entire VP1 subunit. In a 20-ps simulation, VP1 underwent a delocalized movement of 1.14 Å. All atoms showed slight displacement with the largest atomic displacement being 2 Å in Met-205 Cα. In an informative control trajectory, the drug was freed from fixed atom restraint at $\lambda = 0.1$ and allowed to relax over 10 ps. The entire subunit underwent a partial relaxation, returning to within 0.668 Å rms of the initial structure, while the drug moved further down into the binding pocket (away from the surface). If left totally unconstrained, significant deformation occurs over 15 ps; the oxazole–phenoxy (OP) end of the drug moves considerably, ending up hydrogen bonded to a different asparagine residue (Asn-88 of subunit VP1), while the I end remains immobile. Specifically, atom WIN N21, which hydrogen bonds to VP1 Asn-203 in the initial structure, ends hydrogen bonded to VP1 Asn-88.

This would support the hypothesis of strong affinity between these two moieties. Some interesting drug–protein hydrogen bonds were observed. In model 1 at 300 K, the single Asn-203–Win 21 hydrogen bond had a lifetime of 30 ps, while at 1000 K, a novel hydrogen bond was found between Gly-206 NH and WIN O13 (not found at 300 K), which survived through 40 ps and indeed counteracted the growing nonbonded interactions. Many protein–protein hydrogen bonds were observed in residues 196 to 210, but in all simulations, they seemed to be particularly prevalent in the region of residues 199–203. The formation of transient γ-turns and other bends around the two glycine pivot point residues 198 and 206 was also frequently observed, again in all simulations. More *intra*loop hydrogen bonds (within and between residues 196–210) occurred in slow-growth dynamics than did in normal dynamics. In one 50-ps trajectory, the number of hydrogen bonds with slow growth was initially about the same as that of the control simulation, but a transition occurred where the number of hydrogen bonds with slow growth increased by three over the control (see Figure 5).

Two ancillary simulations were performed. These included a sequential-growth model and solvent-comparison model. A sequential-growth simulation using model 2 showed differences from the normal slow-growth trajectories consistent with the change in order of scaling of interactions. The growth of forces from the I end caused heightened evolution of displacements in 203–210 and diminished displacement in the 196–203 region (see Figure 3). Gross solvent considerations were investigated by comparing two otherwise identical 10-ps slow-growth simulations; in one a constant dielectric was used and in the other an r-dependent dielectric. The final structures contained a different number of hydrogen bonds, but the hydrogen bond locations found were exactly co-incident. There were two less in the r-dependent dielectric model, and these occurred in the region between Thr-200 and Asn-203 (Figure 4).

For purposes of comparison, a fully equilibrated (over 100 ps) starting structure[19] was used to assess the slow-growth effect. A 50-ps simulation showed backbone displacement of only 2.38 Å from the native (see Figure

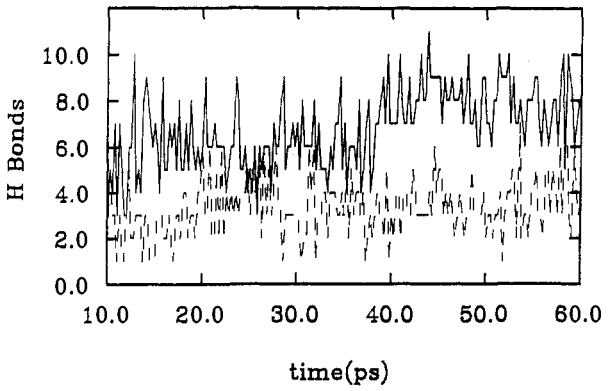

Figure 3. Number of hydrogen-bond interactions as a function of time. Atoms of VP1 196–210 and WIN compound are included in the model 1 calculation. The dashed line depicts the control case with no slow growth.

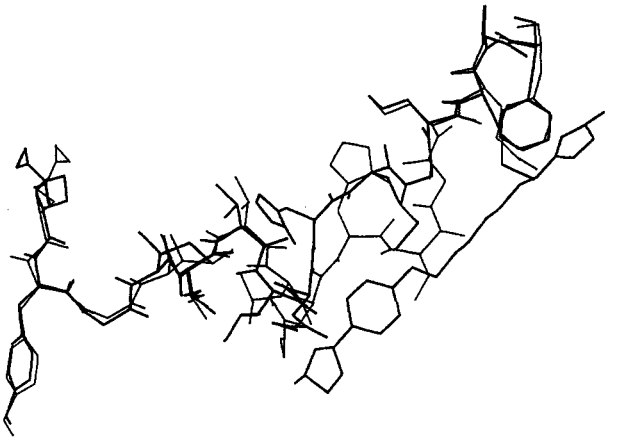

Figure 4. Comparison of the final structure from a sequential growth model simulation of 26 ps (dark) and the minimized apoprotein structure (light). Drug atoms were "grown" from the isoxazole end.

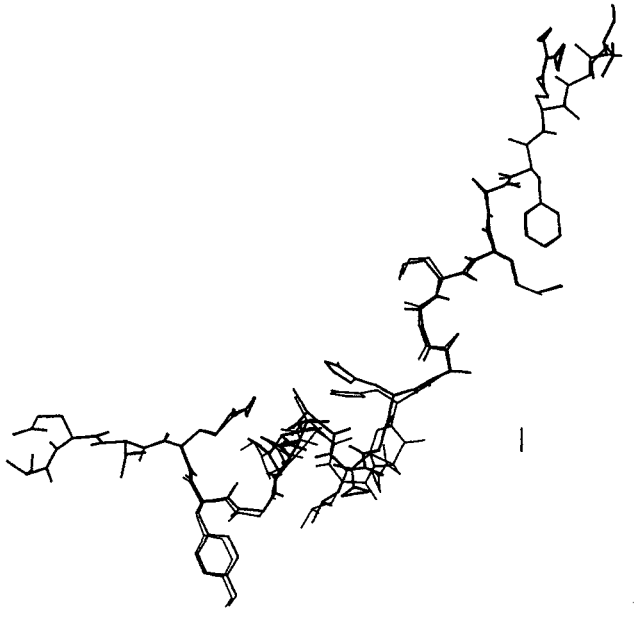

Figure 5. Comparison of final structures from a 10-ps trajectory using a constant dielectric (light) versus an r-dependent dielectric (dark).

6), and the effect of the perturbation was delocalized. The observed displacement, while less than that found using the unequilibrated structure, was essentially localized between the two glycine residues 198 and 206 suggesting a hinge-like region. The increased atomic fluctuations in

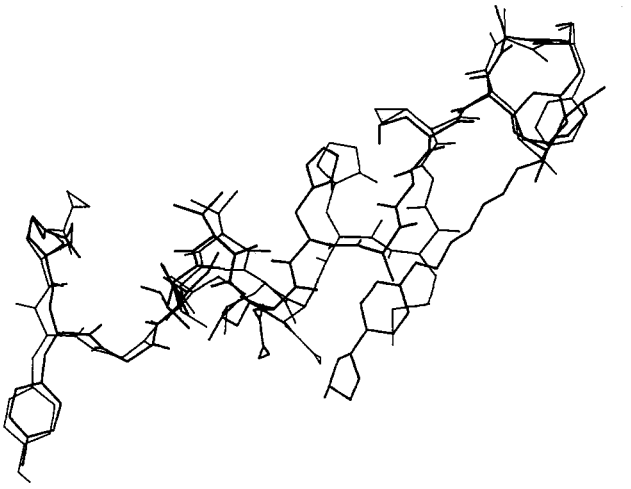

Figure 6. Comparison of initial (light) and final (dark) structures of a slow-growth trajectory using a completely equilibrated apoprotein initial structure. All atoms except those of residues VP1 196–210 were fixed. (Atoms of residues 196–210 and the WIN compound are shown.)

the unequilibrated structure were analogous to those created by a higher temperature (see below).

Examining the simulations, correlating trajectory time and degree of displacement in slow-growth trajectories showed that conformational accessibility of the loop region was not severely limited by the length of the simultion for simulation durations greater than about 30 ps. Root mean square (rms) displacement as a function of time in fact showed a linear relationship. This suggests considerable mobility in the loop during the induced transitions.

Using model 1, high-temperature simulations were performed at 2000 K to force the sampling of a greater portion of the conformational space available to the active-site residues (196–210). At 2000 K backbone displacements of up to 7.7 Å (after quenching) were observed. The greatest movement occurred in residues 196–205, while in 206–210 no backbone displacement greater than 1.5 Å was observed, presumably because this region (206–210) remained kinetically trapped in the VP1 β barrel on this time scale (50 ps). These large atomic excursions of the protein backbone represent conformationally possible but statistically rare events. Mapping of the conformational space around the crystallographic states by this method can identify states of similar energy (±10 kcal/mol) but tells nothing of the activational energy barriers separating them.

Quenching from 2000 K generated a manifold of structures with a range of energies. In other applications of this technique (without slow growth) both an energy sieve as well as geometric similarities between the resulting structures have been used reliably to probe the number of conformations available at lower temperatures (e.g. 300 K) even though the equilibrium constants (populations) yielded by such a search, in general, are not representative of the lower temperatures.[20] Here we adopted the same analysis procedure of ref 20. Without slow growth, the quenched structures adopted conformations with energies (of residues 196–210) ranging from −593. to −472. kcal/mol. Out of 100 structures, there were 17 with energy less than −575. kcal/mol and 5 with energy less than −585. kcal/mol, the latter 5 being structures 2, 4, 5, 16, and 17 out of 100. If initiated with slow growth, the conformational energies ranged from −582. to 4960. kcal/mol. Of these 100 structures, 13 had energies less than −560. kcal/

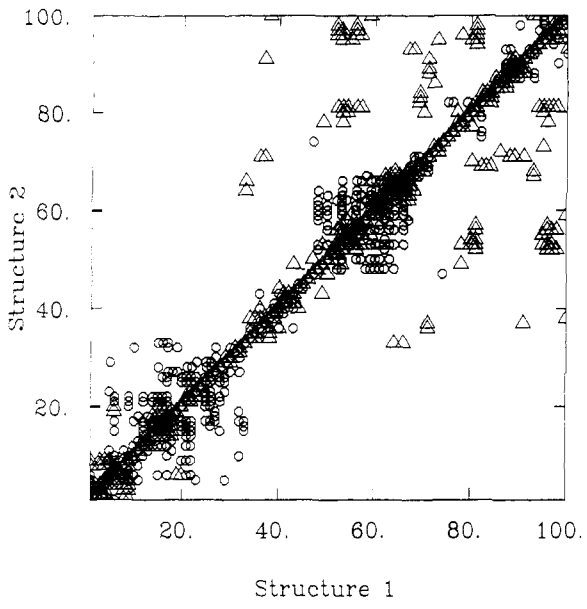

Figure 7. Scatter plot comparison of the 100 structures obtained from periodic quenching of a 50-ps simulation at 2000 K. Maximum allowed rms deviation for residues VP1 196–210 is 2 Å. Triangles indicate quenching of apoprotein; circles indicate quenching of apoprotein coupled with slow growth of WIN compound.

mol and 5 had energies less than −575. kcal/mol, the latter 5 being structures 5, 8, 76, 79, and 82. These structure numbers indicate time of quenching (i.e. structure 100 was quenched at time 50.0 ps in this 50-ps trajectory), and reflect the range of conformational space that the protein has traversed. That low-energy structures exist at points 76, 79, and 82 indicate that low-energy states exist that are far removed from the native crystallographic state.

A scatter plot comparison of the quenched structures, in which all structures with an rms difference of less than 2.0 Å (for residues 196–210) are plotted, is shown in Figure 7. The scatter plot identifies quenched conformations that bear some level of structural similarity. We have shown that similar conformations of the string of "active-site" residues can be reached through minimization from a wide range of conformational space both in the presence and absence of the drug.

As mentioned, quenching in the presence of the drug resulted in five low-energy structures. These five structures were similar in that the β-barrel structure of residues 206–210 was retained, while the conformation of 198–205 varied rather widely with maximum backbone displacements as large as 7.7 Å. Two of these low-energy structures (5 and 8) showed a hydrogen bond between Asn-203 and both the carbonyl O of VP1 Leu-82 and atom WIN N21. The three remaining structures, 76, 79, and 82, showed structural motifs involving VP1 Lys-87 and VP1 Arg-252, in which residues 199–203 hydrogen bonded to the side-chain amino moiety of Lys-87. His-204 O (carbonyl) and Asn-203 O (amide) formed a double hydrogen bond to the epsilon nitrogen of Lys-87. In another structure (82), a third hydrogen bond from Thr-200 O (side chain) to the same epsilon nitrogen was found. This particular lysine residue Lys-87 was thus important in stabilizing the relatively large movement of the loop residues 200–204, which again emphasizes their hydrogen-bonding potential. A large movement of the "active-site" residues is theoretically possible and provides a greater access for entry of the drug into its binding pocket than seen in the available crystal structures.

Conclusions

The simple model of the motions of a portion of the FMDV-loop as the binding flap was shown to be a reasonable model even when compared with induced fluctuations in the entire virion. The forced slow-growth variant of molecular dynamics induced motions in the protein environment at normal temperatures including local backbone motions of up to 3 Å and small changes—ring flips, displacement of side chains, etc.—characteristic of those that might coordinate a binding event or affect nonequilibrium stability. We have applied this method to study the mechanism of binding of the WIN compounds to HRV-14. Only a portion of the conformational space between the two states was sampled; a trajectory ending within less than 1 Å rms of the correct drug-bound structure was not found. We conclude that the ligand-induced transition from apo to holo conformations in the viral capsid protein involves larger or more complex movements than are accessible by our methods (for a given time scale) alone. In our high-temperature trajectories backbone displacements of up to 7.7 Å are found in structures with energies similar to those of the crystallographic states; therefore, a mechanistic model involving larger displacements than 5 Å, such as a "loop-cap" transition, is a more credible possibility. That two glycine residues (VP1 198 and VP1 206), previously implicated[3] as pivot points in the drug-induced displacement, act as hinges in this transition is supported by both the localization of fluctuations between these residues in slow-growth dynamics and the frequent occurrence of transient turns and bends centered around these residues in all simulations. Furthermore, the strong hydrogen bonding potential of residue VP1 Lys-87 might provide a latch by which to fasten Asn-203 and its neighboring residues, thereby creating a larger fluctuating opening to the binding site.

Both the forced slow-growth and high-temperature simulations provide a way to monitor changes in the number and distribution of hydrogen bonds that occur under nonequilibrium conditions. In the region of residues 197–204 of the VP1 subunit, hydrogen bonds seem to have a stabilizing effect. In the extreme temperature simulation of rare (improbable) events, the greatest displacement is observed in these same residues.

The apparent propensity for hydrogen bonding of this surface-exposed region makes it tempting to propose this as the initial recognition site for the drug. The sequence (Gly-Ile-Thr-Val-Leu-Asn) contains approximately the same ratio of polar to nonpolar residues as is found in the drug and may provide a favorable environment for the initial affinity between the drug and virus.

We have observed specific hydrogen bonds which we believe are important at some stage of the binding process of the WIN compound. A hydrogen bond between VP1 Asn-203 and WIN N21 is found in the holo crystallographic structure, but even in the slow-growth trajectories, which use the apoprotein initial coordinates, this same hydrogen bond exists and indeed survives for various times in various simulations with a maximum lifetime of 30 ps. The only other hydrogen bond we observed having a significant lifetime was that between Gly-206 and WIN O13, which survives for 40 ps even at 1000 K. We suggest that the two

drug atoms N21 and O13 are important for the drug's recognition and that the residues 199–204 are clearly important for the binding of the WIN compound. Both of these hypotheses are testable through alternative synthesis and mutagenesis, respectively. The 203 Asn–WIN interaction may be strong enough to function as a "hook" with which to pull the drug into the pocket or at least orient it in certain stages of binding, but other studies have predicted that the 203 Asn–WIN hydrogen bond is not important for final (equilibrium) thermodynamic stability,[7] implying a possible kinetic advantage. Our quenching simulations indicate that the presence of the drug modifies the visitation of certain conformations by the native structure, which could reflect a disturbance of the normal fluctuations or "breathing" of the residues near the binding site and could in turn alter protomeric disassociation in the host cell. It has been postulated that the drug may alternatively function as a "plug" in the ion channel underlying the binding site. Future studies with explicit treatment of solvent molecules will address this question.[19] Our forced slow-growth and high-temperature sampling methods have been used to prove small- to intermediate-scale conformational changes and have the potential of elucidating pharmacologically important aspects of drug–protein interaction.

Acknowledgment. The authors are grateful to acknowledge partial support of this work by the NIH, the Robert A. Welch Foundation, and the Alfred P. Sloan Foundation. Prof. M. Rossmann is thanked for many stimulating conversations that led to the idea for this work. SDSC (initially) and PSC (subsequently) are thanked for computer time. This work was extracted from the senior honors thesis of M.G.B.

References

(1) Rueckert, R. R. *Comprehensive Virology*; New York: Plenum, 1976; Vol. 6, pp 131–213.
(2) Rossmann, M. G.; Arnold, E.; Erickson, J. W.; Frankenberger, E. A.; Grittith, J. P.; Hecht, H. J.; Johnson, J. E.; Kamer, G.; Luo, M.; Mosser, A. G.; Rueckert, R. R.; Sherry, B.; Vriend, G. *Nature* **1985**, *317*, 145–153.
(3) Smith, T. J.; Kremer, M. J.; Luo, M.; Vriend, G.; Arnold, E.; Kamer, G.; Rossmann, M. G.; McKinlay, M. A.; Diana, G. D.; Otto, M. J. *Science* **1986**, *233*, 1286–1293.
(4) Wilfert, C. M.; Zeller, J. R.; Schanber, L. E.; McKinner, R. E. 24th Interscience Conference on Antimicrobial Agents and Chemotherapy, Washington, D.C., 1984; Abstract 430.
(5) Branden, C.; Tooze, J. *Introduction to Protein Structure*; Garland Publishing Co.: New York, 1991.
(6) Badger, J.; Minor, I.; Kremer, M. J.; Oliveria, M. A.; Smith, T. J.; Griffith, J. P.; Guerin, D. M. A.; Kirshnaswamy, S.; Luo, M.; Rossmann, M. G.; McKinlay, M. A.; Diana, G. D.; Dutko, F. J.; Fancher, M.; Rueckert, R. R.; Heinz, B. A. *Proc. Natl. Acad. Sci. U.S.A.* **1988**, *85*, 3304–3308, and private communications with the authors.
(7) Lau, W. F.; Pettitt, B. M.; Lybrand, T. P. *Mol. Sim.* **1988**, *1*, 385–398.
(8) Diana, G. D.; Oglesby, R. C.; Akullian, V.; Carabateas, P. M.; Cutliffe, D.; Mallamo, J. P.; Otto, M. J.; McKinlay, M. A.; Maliski, E. G.; Michalec, S. J. *J. Med. Chem.* **1987**, *30*, 383–393.
(9) See numerous papers in: *Computer Simulation of Biomolecular Systems: theoretical and experimental applications*; van Gunsteren, W. F., Weiner, P. K., Eds.; ESCOM Science Publishers: Leiden, 1989.
(10) Wong, C. F.; McCammon, J. A. *J. Am. Chem. Soc.* **1986**, *108*, 3830–3832.
(11) Lybrand, T. P.; McCammon, J. A.; Wipff, A. *Proc. Natl. Acad. Sci. U.S.A.* **1986**, *83*, 833–835.
(12) Wade, R. C.; McCammon, J. A. *J. Mol. Biol.* **1992**, *225*, 697–712.
(13) McQuarrie, D. A. *Statistical Mechanics*; Harper & Row: New York, 1976.
(14) Brooks, B. R.; Bruccoleri, R.; Olafson, B.; States, D.; Swamanithan, S.; Karplus, M. *J. Comput. Chem.* **1983**, *4*, 187–217; with S. Fleischman and C. Brooks, perturbation code.
(15) Diana, G. D.; McKinlay, M. A.; Otto, M. J.; Akullian, V.; Oglesby, C. *J. Med. Chem.* **1985**, *28*, 1906–1910.
(16) Verlet, L. *Phys. Rev.* **1967**, *159*, 98–103.
(17) Wade, R. C.; McCammon, J. A. *J. Mol. Biol.* **1992**, *225*, 679–696.
(18) Holder, M.; Biswas, M.; Pettitt, B. M. Unpublished results.
(19) Oconnor, S.; Smith, P. E.; Al-Obeidi, F.; Pettitt, B. M. *J. Med. Chem.* **1992**, *35*, 2870–2881.